

Search for Pauli Exclusion Principle Violations with Gator, a High-Purity Germanium Detector at LNGS

L. Baudis, R. Biondi, A. Bismark, A. Clozza, C. Curceanu, M. Galloway,
F. Napolitano, K. Piscicchia, A. Porcelli, F. Piastra, D. Ramírez García

Trento, June 2024



Universität
Zürich^{UZH}



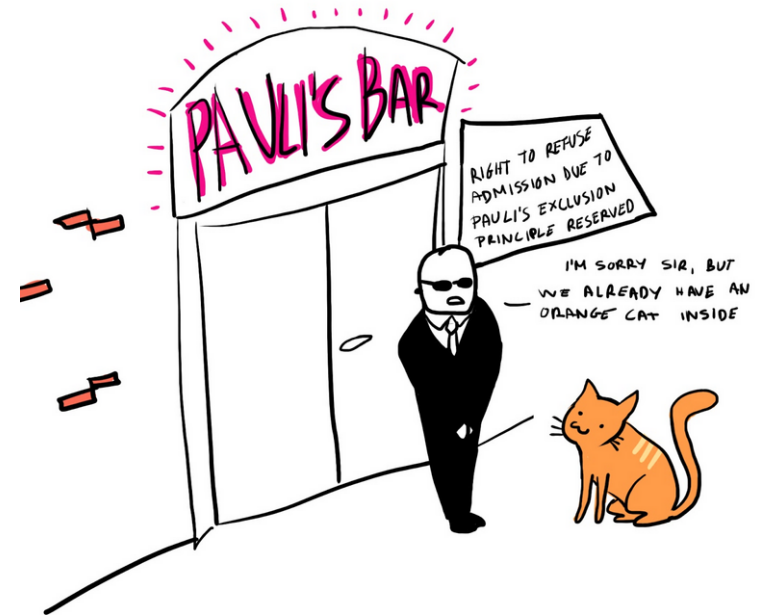
Pauli Exclusion Principle Violations

→ talk by Kristian Piscicchia

- Small violations of the Pauli Exclusion Principle suggested by physics beyond the Standard Model
- Possibility: altered particle properties, e.g., quon model [Phys. Rev. Lett. 59 (1987) 2507]:

$$a_k a_l^\dagger - q a_l^\dagger a_k = \delta_{k,l}$$

- Subject to Messiah-Greenberg superselection rule [Phys. Rev. 136 (1964) B248]
→ can only be tested with open systems
- Typically classification of novelty of the fermion-system interaction (Type I – III) [Found Phys 42 (2012) 1015]

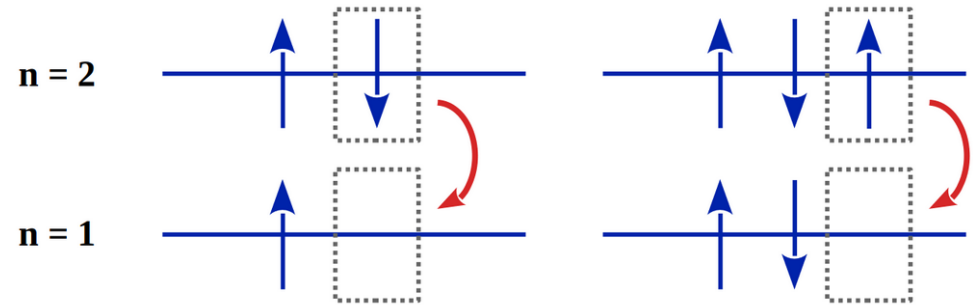


<https://dingercatadventures.blogspot.com/>

Ramberg-Snow Technique

→ talk by Kristian Piscicchia

- Search for anomalous X-ray transitions performed by electrons introduced in a target through a direct current (Type II)
 - lower energy PEP-forbidden transition due to screening of nucleus



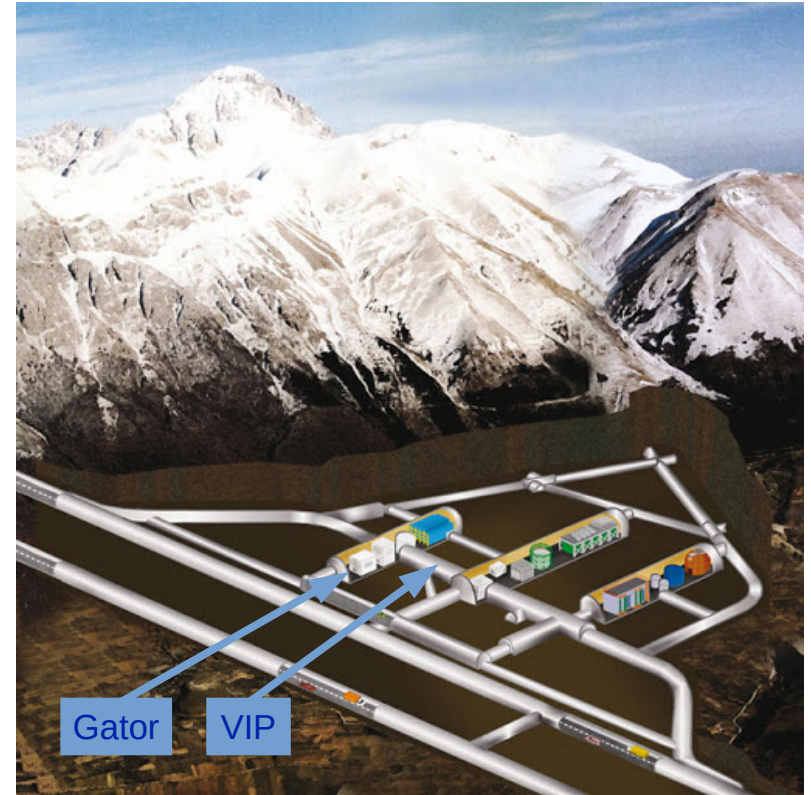
- Technique pioneered by Ramberg and Snow [Phys. Lett. B 238 (1990) 438]; presently strongest limit on $\beta^2/2$ by VIP-2 experiment with Cu conductor [Symmetry 14 (2022) 893]
- Importance of testing the PEP violation probability for various elements
 - here: investigate for Pb
 - previous best limit with Ge detector: $\beta^2/2 < 1.5 \cdot 10^{-27}$ [Found Phys 42 (2012) 1015]

Transition	EM energy	PEPV energy
1s - 2p _{3/2} K _{α1}	74.969 keV	73.713 keV
1s - 2p _{1/2} K _{α2}	72.805 keV	71.652 keV

The Gator Facility

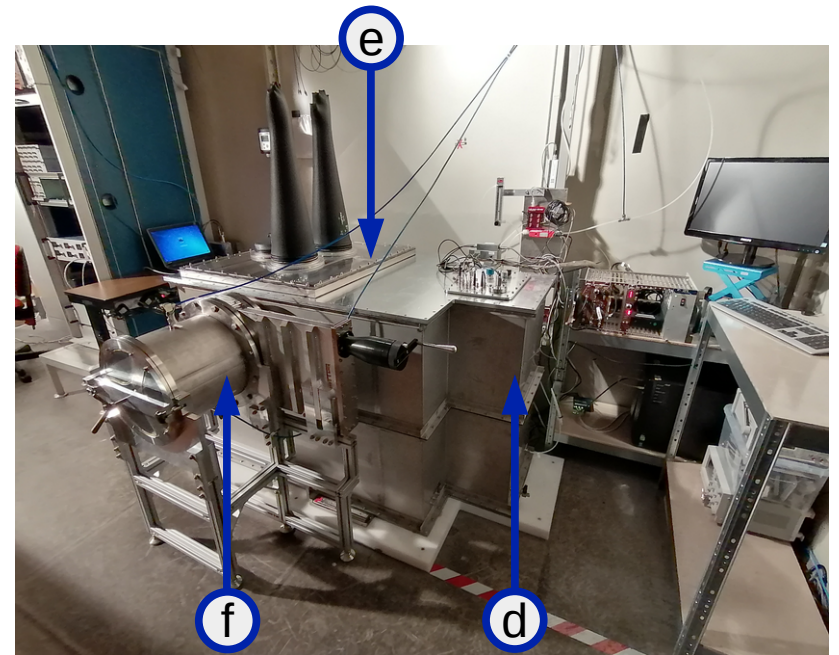
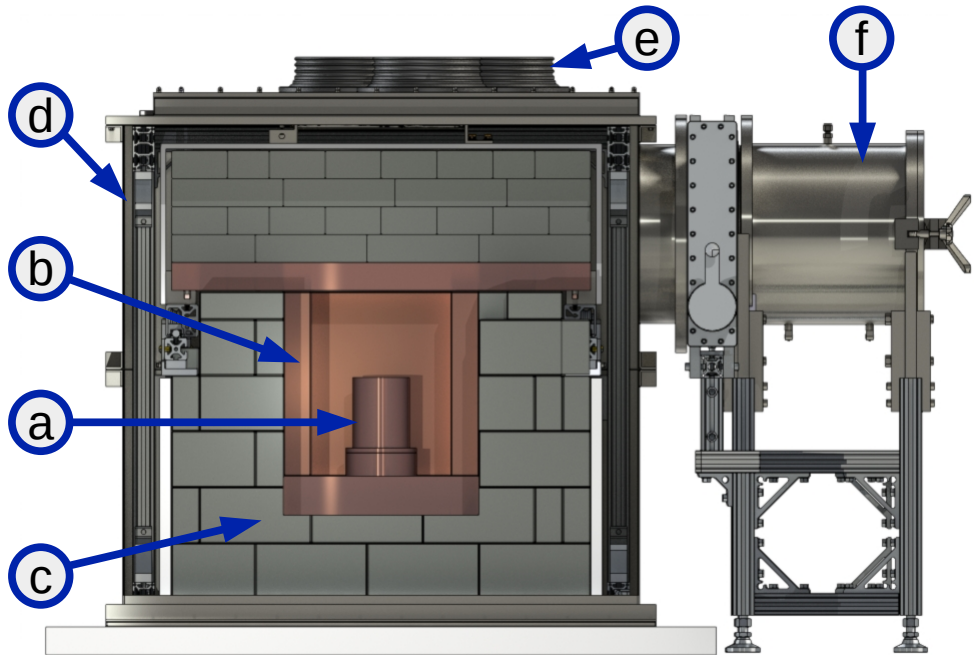
→ JINST 17 (2022) P08010

- Low-background germanium counting facility for high-sensitivity γ -ray spectrometry
- Located at the Gran Sasso underground laboratory in Italy (LNGS) at a depth of 3600 m water equivalent
- Core: p-type coaxial high-purity germanium (HPGe) detector with 2.2 kg sensitive mass and a relative efficiency of 100.5%
- Sample chamber volume: $25 \times 25 \times 33 \text{ cm}^3$
- Currently used for material radioassay for rare-event search experiments in astroparticle physic (DARWIN/XLZD, LEGEND,...)



The Gator Detector

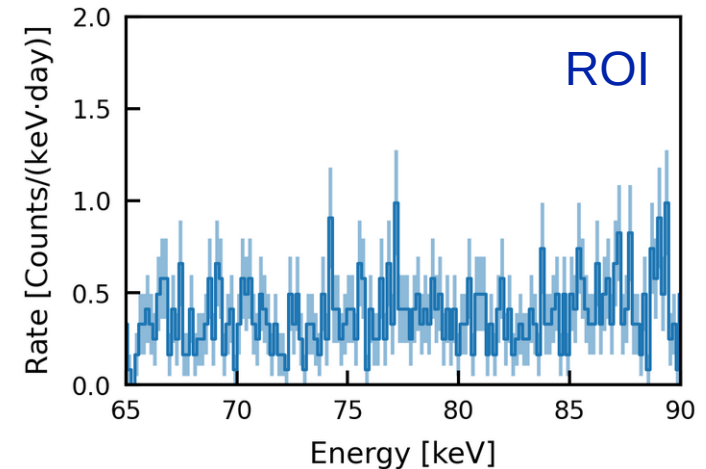
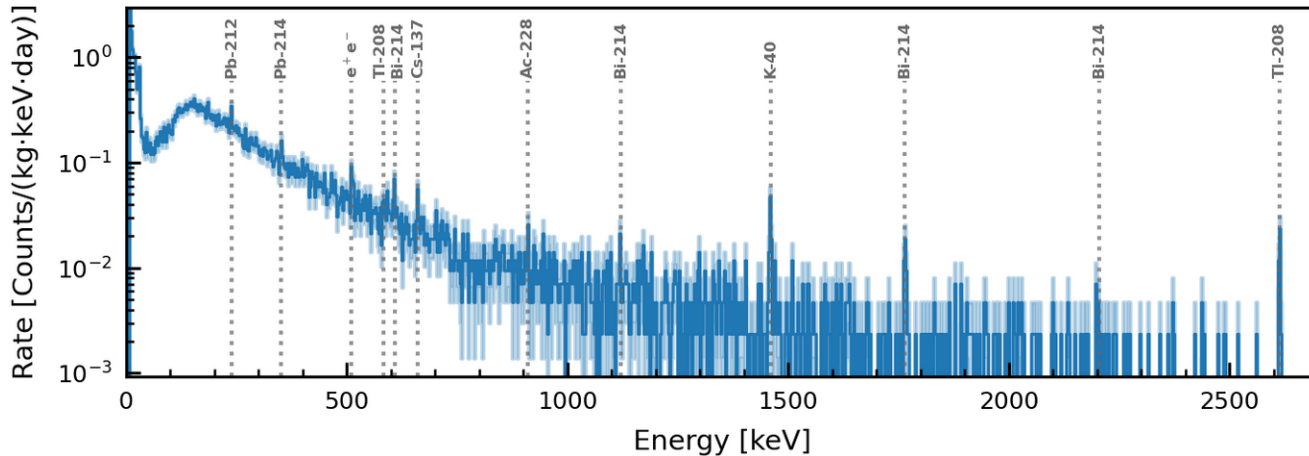
→ JINST 17 (2022) P08010



(a) HPGe detector inside Cu-OFE cryostat (cooled with LN₂ via copper coldfinger), **(b)** OFHC Cu cavity, **(c)** lead shield, polyethylene sheet, **(d)** airtight stainless steel enclosure (purged with GN₂), **(e)** glove ports, **(f)** sample load lock

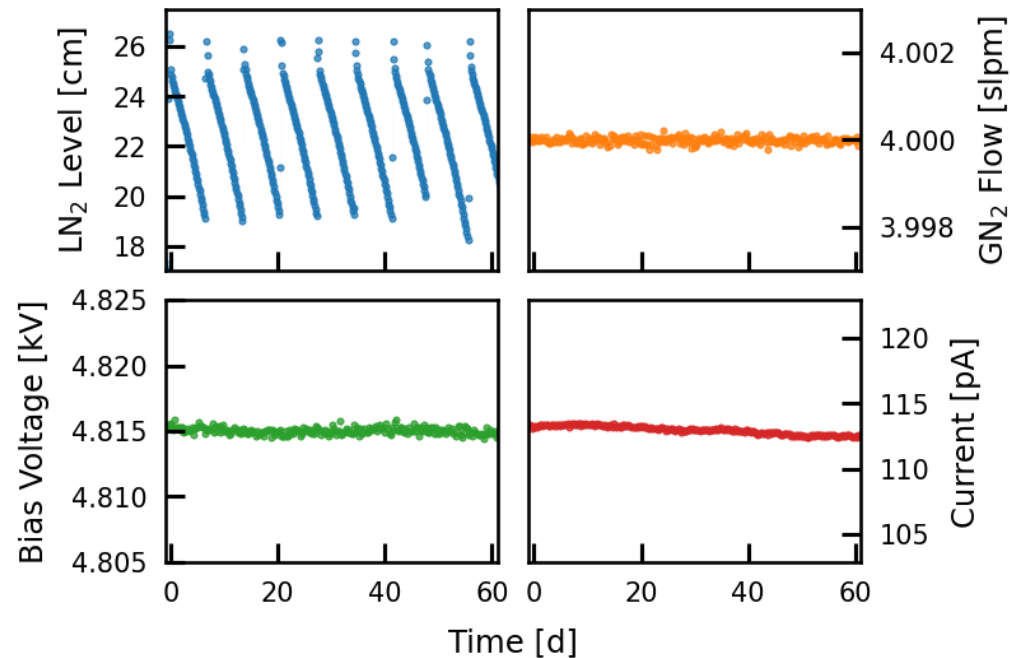
Strength: Low Background

- Main contributions:
 - detector & shielding materials (^{226}Ra , ^{228}Th , ^{40}K , ^{60}Co ,...)
 - environmental radon (^{222}Rn in air)
- Integrated rate in range
 - 100-2700 keV: $(82.0 \pm 0.7) \text{ d}^{-1} \text{ kg}^{-1}$
 - 65-90 keV: $(4.4 \pm 0.3) \text{ d}^{-1} \text{ kg}^{-1}$



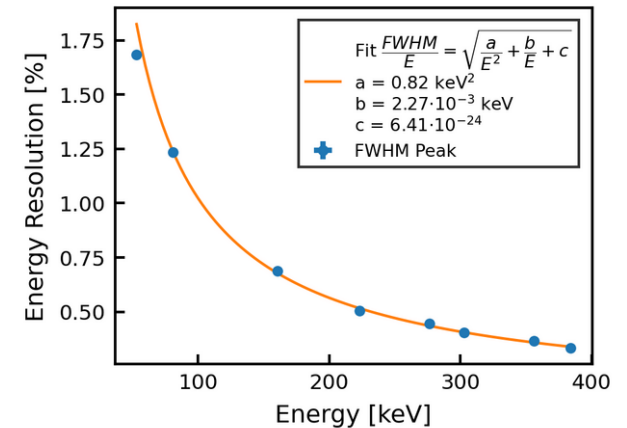
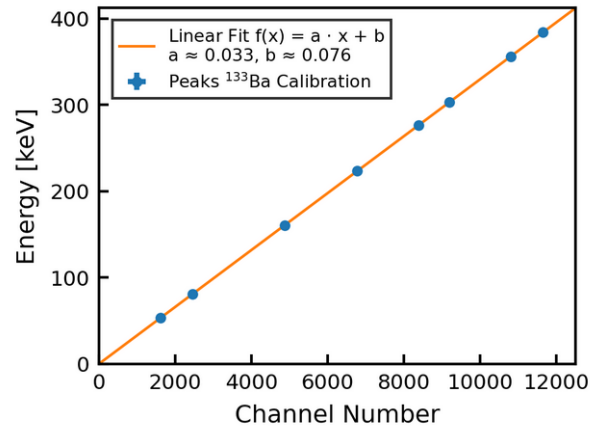
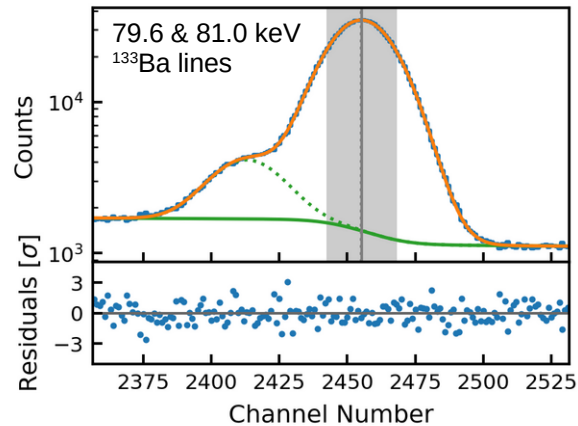
Data Acquisition and Slow Control

- Preamplified signal read out through
 - Ortec Model 672 spectroscopy amplifier and
 - self-triggering Ortec Model ASPEC-927 MCB
- record MCA spectra in 4h intervals (no pulse information available)
- Slow control monitoring operation parameters (HV, I_{leakage} , LN₂ level, temperature, rate,...)
 - detector stability + data quality, removal refill-induced noise

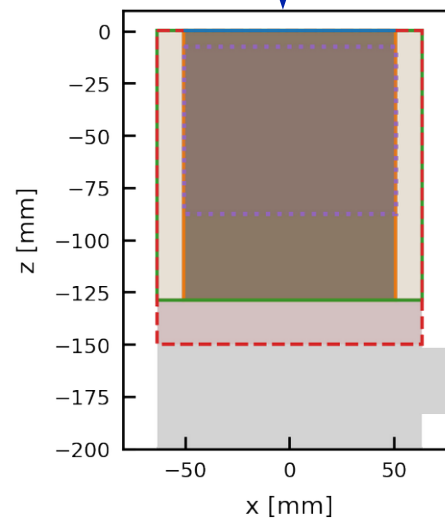
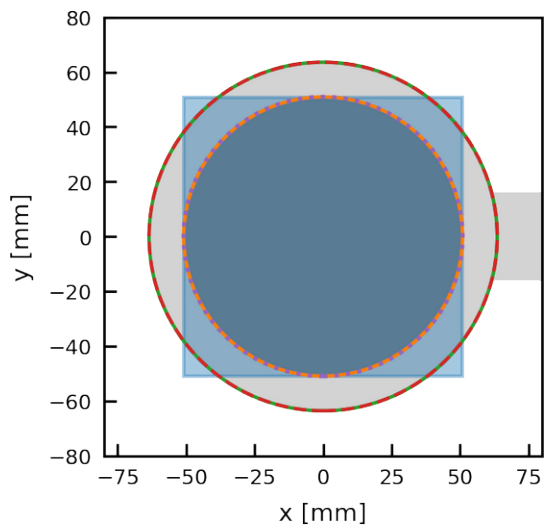
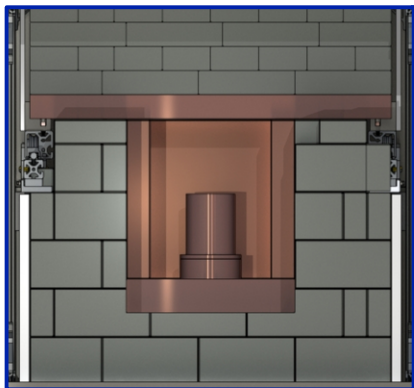


Energy Scale and Resolution

- Regular calibrations with ^{133}Ba and ^{228}Th sources
→ monitoring stability response, verification MC simulations
- Energy range 0 – 540 keV (factor 5 reduction w.r.t. material radioassay)
- Linear energy scale with ~ 0.033 keV/channel
- Resolution ~ 1.0 keV (FWHM) at Pb K_α lines



GEANT4 MC Simulations – Pb Conductor Geometry

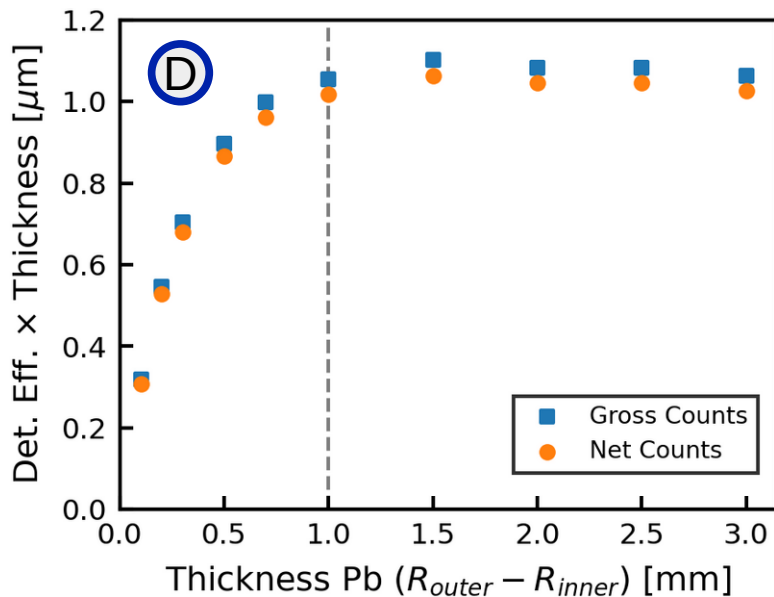
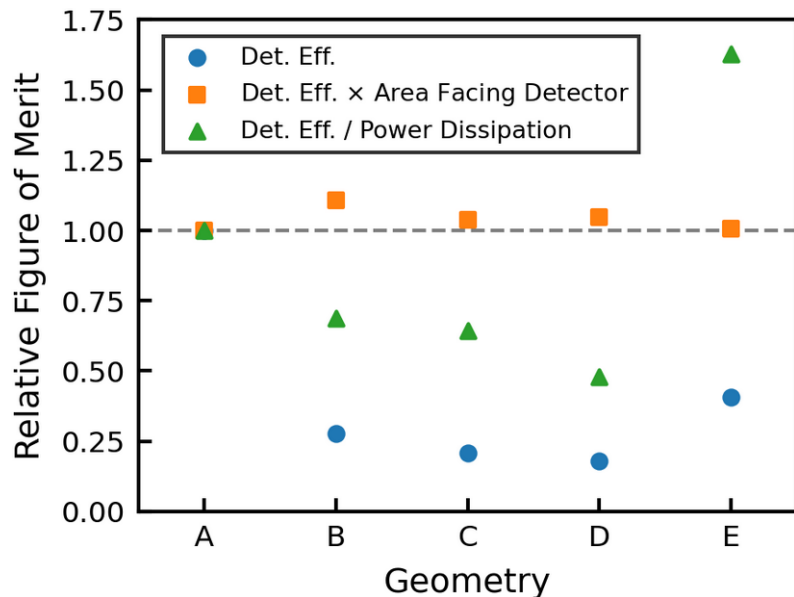


- Cu Cryostat Endcap:
 - $D_{outer} = 101.6$ mm
 - $\Delta z = 129.05$ mm
- Cu Cryostat Base (+ Coldfinger):
 - $D_{outer} = 127.0$ mm
- Hollow Cylinder:
 - $D_{inner} = 101.8$ mm
 - $\Delta z = 129.05$ mm
- Hollow Cylinder:
 - $D_{inner} = 127.2$ mm
 - $\Delta z = 129.05$ mm
- Hollow Cylinder:
 - $D_{inner} = 127.2$ mm
 - $\Delta z = 150.0$ mm
- Hollow Cylinder:
 - $D_{inner} = 127.2$ mm
 - $\Delta z = 79.8$ mm (Sensitive Vol. Sim.)
- Plate:
 - $\Delta x = \Delta y = 101.6$ mm



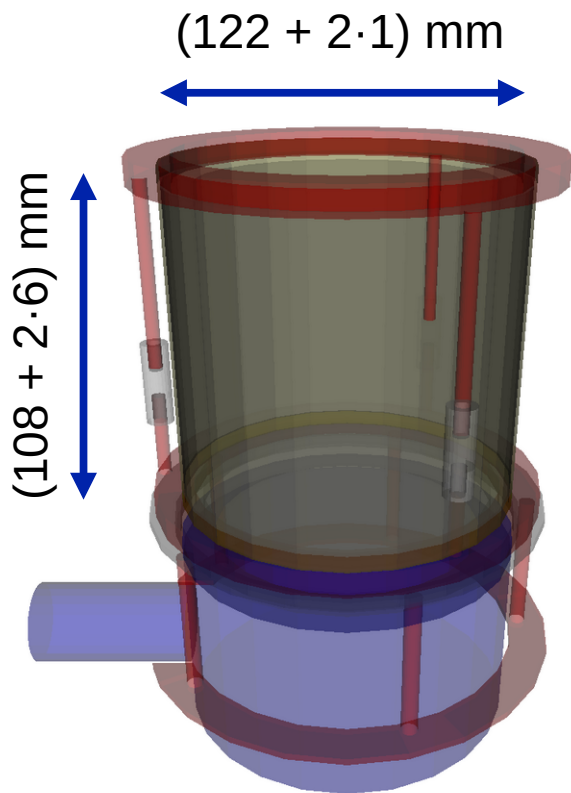
GEANT4 MC Simulations – Geometry + Thickness

Investigate impact Pb conductor geometry and thickness on detection efficiency:

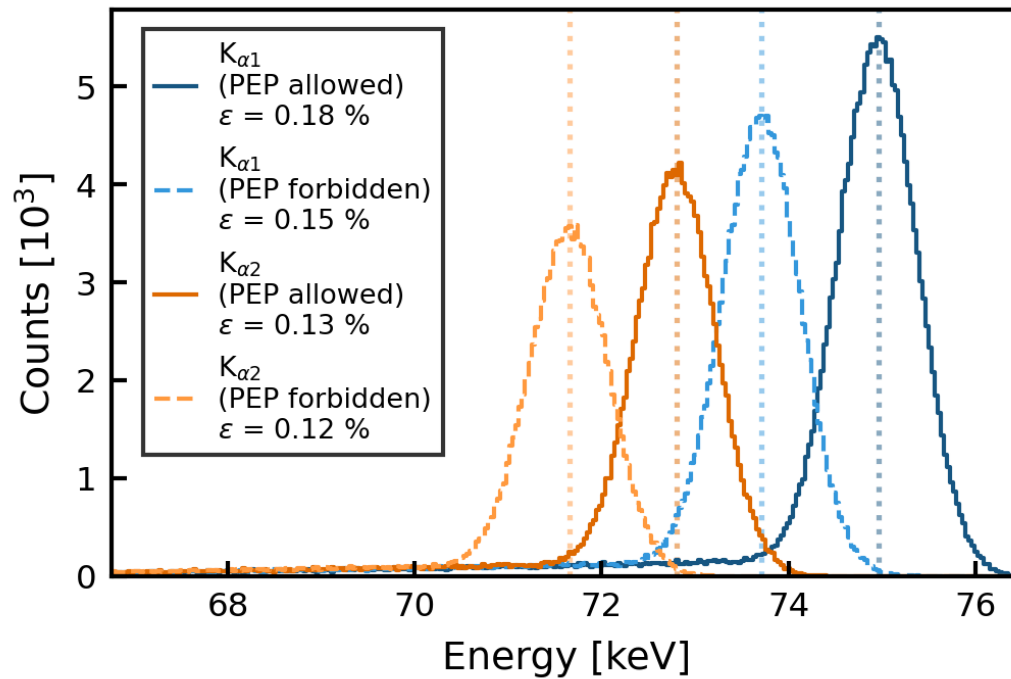


→ Select cylinder geometry with 1 mm wall thickness

GEANT4 MC Simulations – Final Geometry

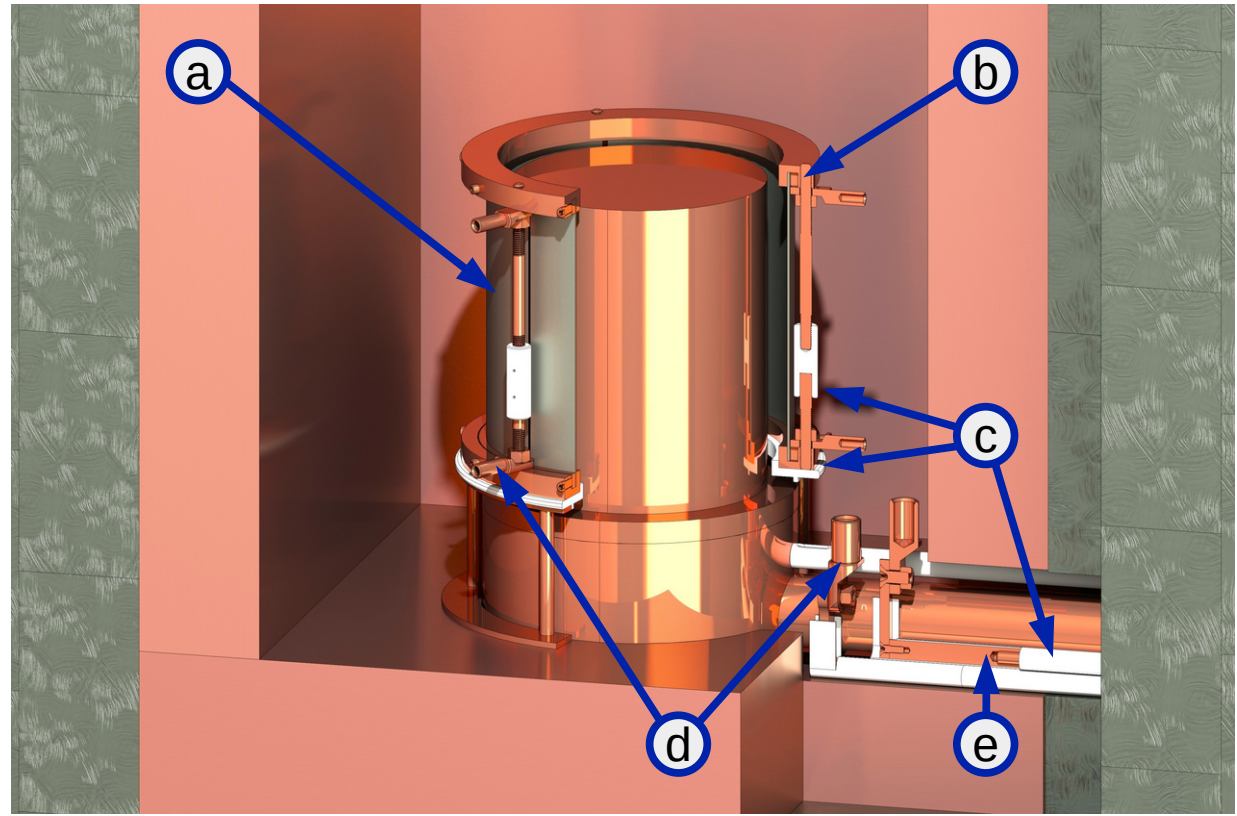


Absorption-induced energy dependence
detection efficiency ε :

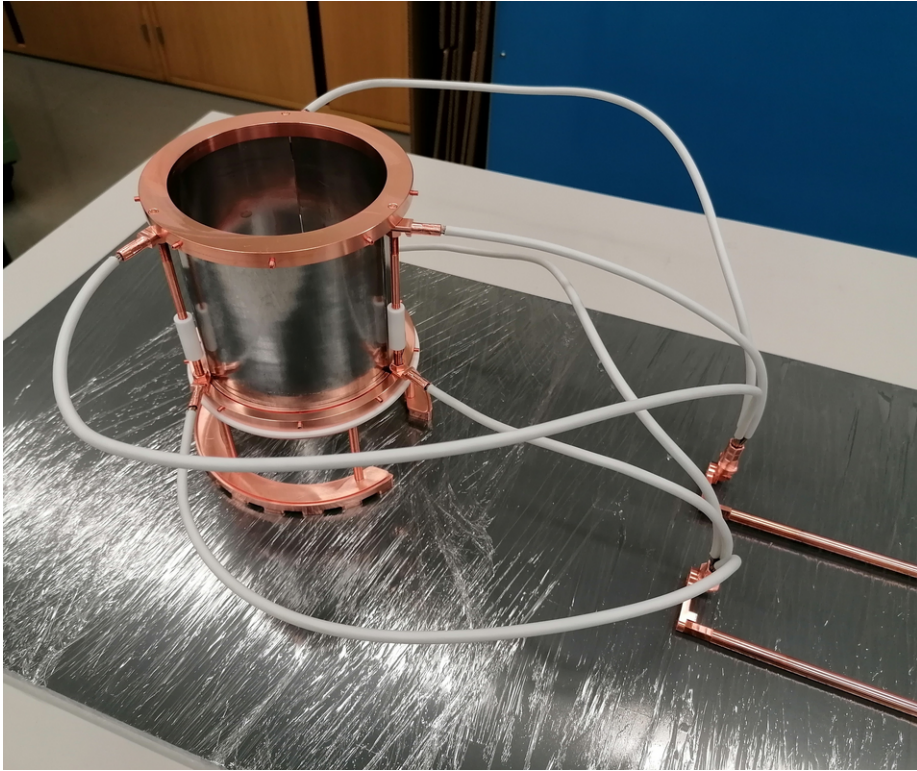


Target Geometry

- (a)** Tripartite Pb foil cylinder
- (b)** Copper rings with segmented clamping elements + set screws
- (c)** PTFE insulation
- (d)** Copper cable lugs for 2 sets of 3 cables each (10 mm², not shown)
- (e)** Segmented high current feedthrough rod



Target Geometry (Photographs)



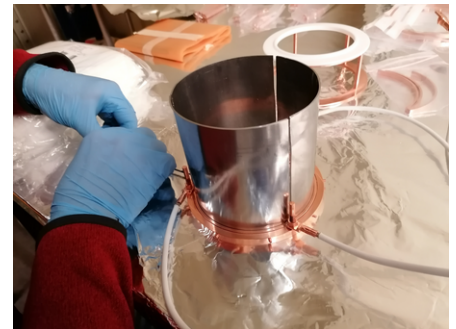
Test assembly at UZH



Inside Gator cavity

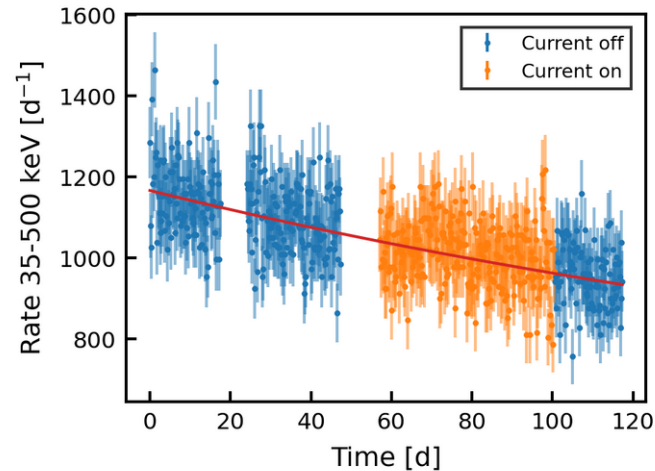
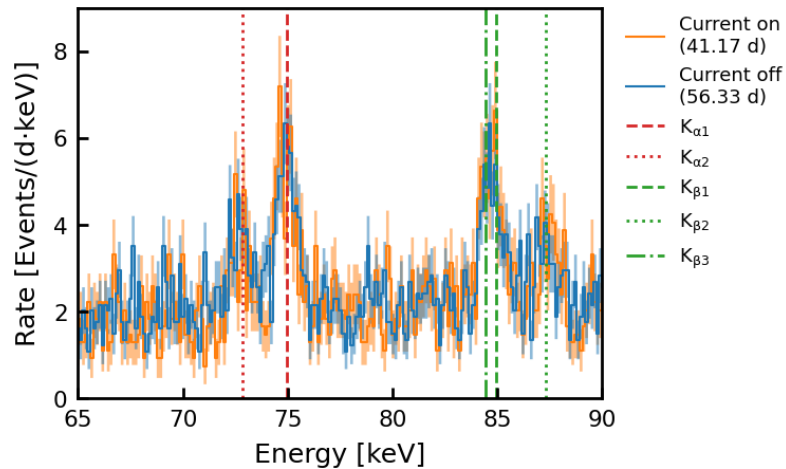
Low-Activity Materials

- Material selection:
 - Custom cast and rolled Roman lead sheets from Lemer Pax with <0.2 Bq/kg
 - Oxygen-free high-conductivity copper from XENONnT array support plate [Eur.Phys.J.C 82 (2022) 7, 599]
 - PTFE plates from XENON1T [Eur.Phys.J.C 77 (2017) 12, 890]
 - Tinned fine-strand copper conductor solar cables
→ material radioassay with Gator
- Minimize component mass to suppress radioactive background; still ensure mechanical stability (→ SolidWorks simulations) and sufficient conductor cross-sectional and surface areas to reduce heat-up (→ calculations + thermal tests)



Measurements

- Data taking April – August 2023:
 - 41.17 d current ON (40 A DC from current-stabilized Agilent N5761A Power Supply)
 - 56.33 d current OFF (as background reference)
- Time-dependent background rate from activated radioisotopes
→ expected 5–7% mean rates difference



Analysis – General Assumptions

- Investigate PEP-violating $K_{\alpha 1}$ (BR = 0.47) and $K_{\alpha 2}$ (BR = 0.23) lines
- Total number of interacting new electrons taken as

$$N_{CE} = \frac{I \cdot \Delta t}{e} \cdot \frac{D}{\mu} \cdot P_{cpt}$$

with - $I = 40$ A (current)

- $\Delta t = 41.17$ d (current-on live time)

- $e = 1.602 \cdot 10^{-19}$ C (elementary charge)

} # introduced current electrons

- $D = 10.8$ cm (effective length Pb conductor)

- $\mu = 2.34 \cdot 10^{-7}$ cm (mean free path current electron in Pb)

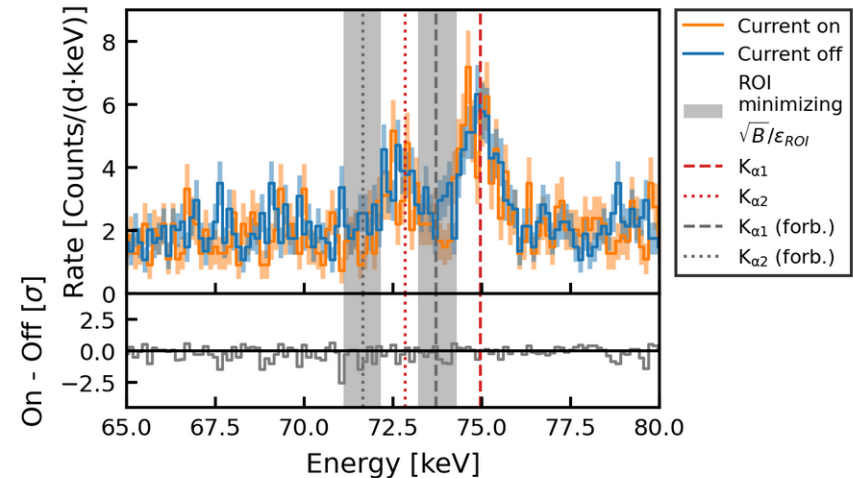
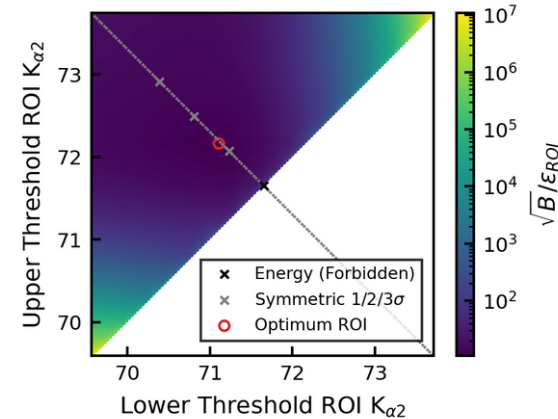
} # electron-atom interactions per e^-

- $P_{cpt} = 0.9\%$ (electron capture probability)

Analysis – Simple Counting Method

- Estimate following [Found Phys 42 (2012) 1015] for comparability
- Gross difference On – Off in ROI minimizing \sqrt{B}/ϵ_{ROI} :
 $N_{\alpha 1} = -(16 \pm 14)$ cnts $\equiv (9 \pm 8)\%$; $N_{\alpha 2} = -(19 \pm 12)$ cnts $\equiv (14 \pm 9)\%$
 → time dependence background + local underfluctuation
 → assume vanishing difference for conservative estimate
- Current-off livetime corrected, weighted average net count Poisson error yields 3σ upper limit electron-atom interactions $N_{3\sigma}/\epsilon_{tot} \approx 3 \times 1.65 \cdot 10^4$ (with ϵ_{tot} including $\epsilon_{detection}$, BR, and ϵ_{ROI})
- Resulting limit factor ~ 11 improvement:

$$\frac{1}{2} \beta^2 < \frac{N_{3\sigma}}{\epsilon_{tot} \cdot N_{CE}} = 1.3 \cdot 10^{-28}$$



Analysis – Fitting

- Background / signal model:

$$\mathcal{F}(\boldsymbol{\theta}, \mathbf{y}, \mathcal{S}) = y_1 \cdot K_{\alpha_1}(\theta_1, \theta_2) + y_2 \cdot K_{\alpha_2}(\theta_3, \theta_4) + y_3 \cdot \text{Pol}_1(\theta_5) + \mathcal{S} \cdot \varepsilon_{det,1} \cdot \varepsilon_{BR,1} \cdot \text{PEPV}_1(\theta_2) + \mathcal{S} \cdot \varepsilon_{det,2} \cdot \varepsilon_{BR,2} \cdot \text{PEPV}_2(\theta_4)$$

PEP-allowed peaks (points to $y_1 \cdot K_{\alpha_1}(\theta_1, \theta_2) + y_2 \cdot K_{\alpha_2}(\theta_3, \theta_4)$)

Background continuum (points to $y_3 \cdot \text{Pol}_1(\theta_5)$)

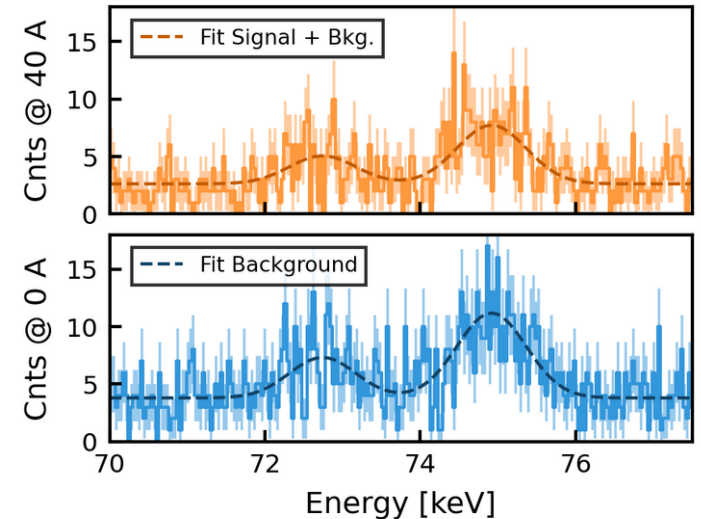
PEP-violating peaks (points to $\mathcal{S} \cdot \varepsilon_{det,1} \cdot \varepsilon_{BR,1} \cdot \text{PEPV}_1(\theta_2) + \mathcal{S} \cdot \varepsilon_{det,2} \cdot \varepsilon_{BR,2} \cdot \text{PEPV}_2(\theta_4)$)

- Likelihood for simultaneous fit:

$$\mathcal{L}(\mathcal{D}^{on}, \mathcal{D}^{off} | \boldsymbol{\theta}, \mathbf{y}, \mathcal{S}) = \text{Pois}(\mathcal{D}^{on} | \mathcal{F}^{on}(\boldsymbol{\theta}, \mathbf{y}, \mathcal{S})) \cdot \text{Pois}(\mathcal{D}^{off} | \mathcal{F}^{off}(\boldsymbol{\theta}, \mathbf{y} \cdot \mathcal{R}))$$

- Empirical normalization factor:

$$\mathcal{R} = \int_{\mathcal{D}^{on}} \int_E f dt dE / \int_{\mathcal{D}^{off}} \int_E f dt dE$$



Results – Fitting (Bayesian)

- Gaussian priors for θ (\rightarrow calibrations) and \mathbf{R} (\rightarrow background time-dependence, $t^{\text{on}}/t^{\text{off}}$)

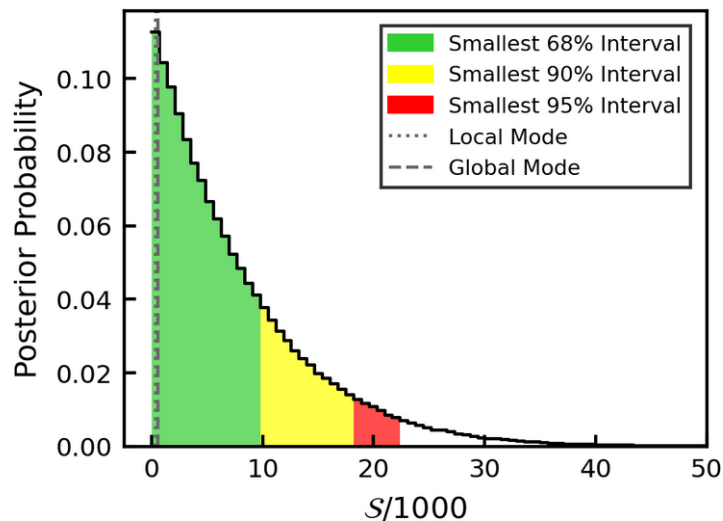
- Posterior probability:
$$p(\theta, \mathbf{y}, \mathcal{S} | \mathcal{D}^{\text{on}}, \mathcal{D}^{\text{off}}) = \frac{\mathcal{L}(\mathcal{D}^{\text{on}}, \mathcal{D}^{\text{off}} | \theta, \mathbf{y}, \mathcal{S}) p(\theta, \mathbf{y}, \mathcal{S})}{\int \mathcal{L}(\mathcal{D}^{\text{on}}, \mathcal{D}^{\text{off}} | \theta, \mathbf{y}, \mathcal{S}) p(\theta, \mathbf{y}, \mathcal{S}) d\theta d\mathbf{y}}$$

- Marginalized posterior probability distribution of signal yield \mathcal{S} via MCMC integration:

$$p(\mathcal{S} | \mathcal{D}^{\text{on}}, \mathcal{D}^{\text{off}}) = \int p(\theta, \mathbf{y}, \mathcal{S} | \mathcal{D}^{\text{on}}, \mathcal{D}^{\text{off}}) d\theta d\mathbf{y}$$

- Mode at $\mathcal{S} = 0 \rightarrow$ upper limits using $\beta^2/2 = \mathcal{S}/N_{\text{CE}}$:

- 90% C.L.: $\mathcal{S} < 1.84 \cdot 10^4 \rightarrow \beta^2/2 < 4.8 \cdot 10^{-29}$
- 99% C.L.: $\mathcal{S} < 32.9 \cdot 10^4 \rightarrow \beta^2/2 < 8.7 \cdot 10^{-29}$



Results – Fitting (Frequentist)

- Cross-check with modified frequentist CL_s analysis
- Exclusion requirement at nominal C.L. of $1-\alpha$:

$$CL_s = \frac{p_S}{1 - p_0} < \alpha$$

with p-value:

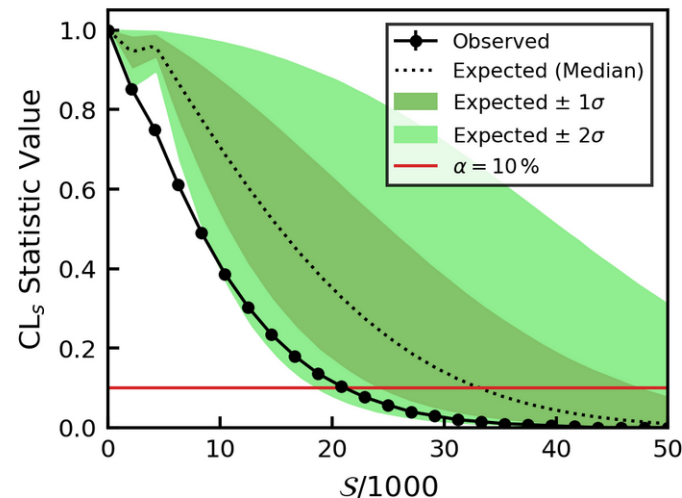
$$p_S = P(t_S \geq t_{obs} | \mathcal{S}) = \int_{t_{obs}}^{\infty} f(t_S | \mathcal{S}) dt_S$$

- Resulting 90% C.L. upper limit ($\alpha = 0.1$) of

$$\mathcal{S} < 2.1 \cdot 10^4 \rightarrow \beta^2/2 < 5.7 \cdot 10^{-29}$$

slightly more conservative than Bayesian approach

- $\sim 1.5\sigma$ deviation from the median expected CL_s statistic



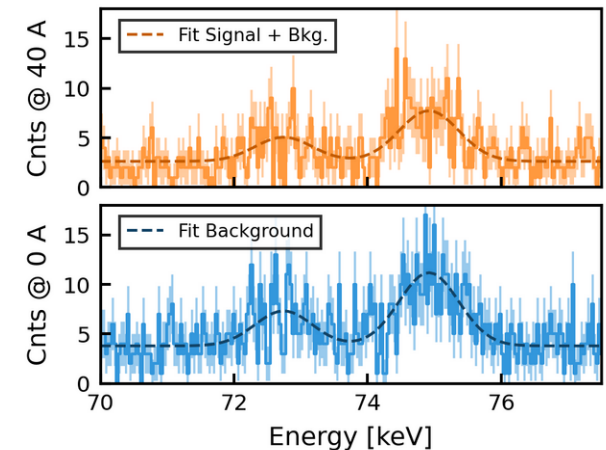
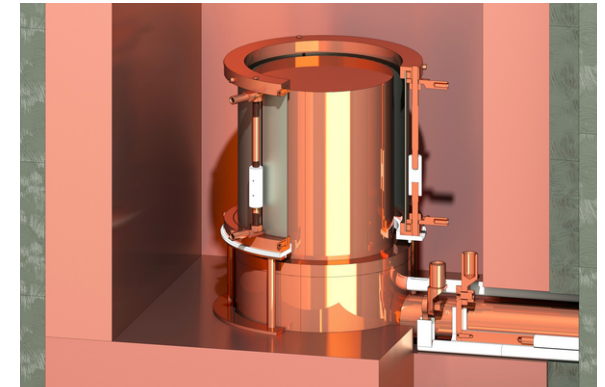
Summary and Conclusion

→ Manuscript in preparation

- Search for small Pauli Exclusion Principle violations with Gator, a low-background HPGe detector at LNGS
- Applied Ramberg-Snow technique to probe PEP-forbidden $K_{\alpha 1}$ and $K_{\alpha 2}$ transitions in a current-carrying Pb conductor in compliance with the Messiah-Greenberg superselection rule (type II experiment)
- No signs of PEP violations observed
→ set limits improving previous most stringent bounds for this type of measurement and material by more than one order of magnitude:

$$\frac{1}{2} \beta^2 < 4.8 \cdot 10^{-29}$$

Bayesian analysis (90% C.L.)



Appendix

Novelty Fermions

- Categorization experiments by how “new” the fermion-system interaction can be assumed to be according to [Found Phys 42 (2012) 1015]:
 - **Type I:** fermion has not previously interacted with any other fermions
 - primordial system formation
 - recently created fermions, e.g., from β -decay or pair production (Type Ia)
 - **Type II:** fermion has not previously interacted with that investigated system
 - distant fermions brought to interact with system, e.g., Ramberg-Snow technique employed here
 - nearby fermions brought to interact with system, e.g., electrons in the Fermi sea of a conductor (Type IIa)
 - **Type III:** fermion within investigated system
 - violate the MG superselection rule, but can set stringent bounds on the spin-statistics deformation induced by Non-Commutative Quantum Gravity models

Comparison to Other HPGe Spectrometers

Detector	Location (Depth m.w.e.)	Mass [kg]	Efficiency [%]	FWHM [keV]	Rate 60-2700 keV [cnts/(kg·day)]	Ref.
Gator	LNGS (3600)	2.2	100.5	1.98	89.0 ± 0.7	
Maeve	SURF (4300)	2.0	85	3.19	956.1	[1]
GeMPI 3	LNGS (3600)	2.2	98.7	2.20	24 ± 1	[2]
Belmont	Boulby (2805)	3.2	160	1.92	135.0	[1]
GeOroel	LSC (2450)	2.2	109	1.85	165.3	[3]
GeMSE	LVdA (620)	2.0	107.7	1.96	88 ± 1	[4]

[1] Eur. Phys. J. C 80 (2020) 1044

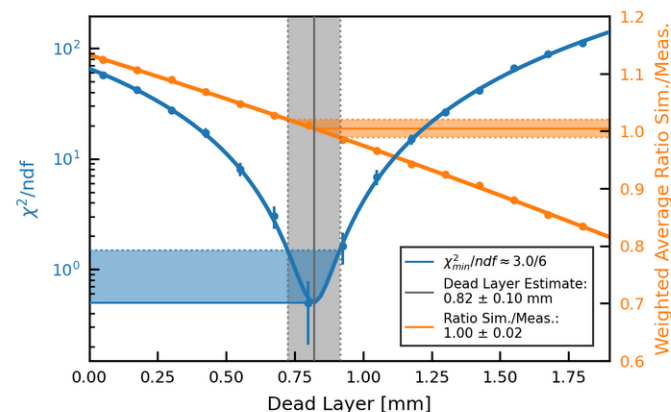
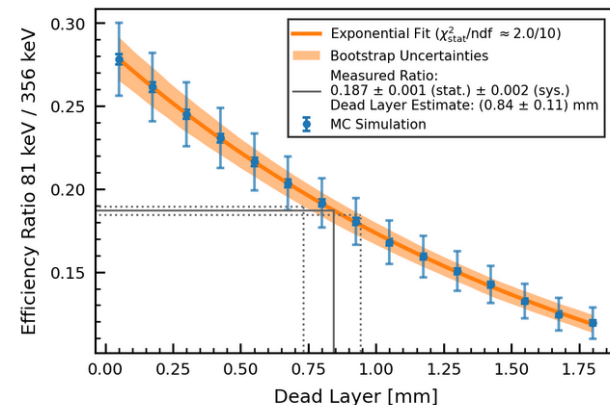
[2] N. Ackermann, private communication

[3] Bandac, "Ultra-Low Background Services in the LSC", DS-Mat Meeting, GSSI, 2019

[4] JINST 17 (2022) P04005

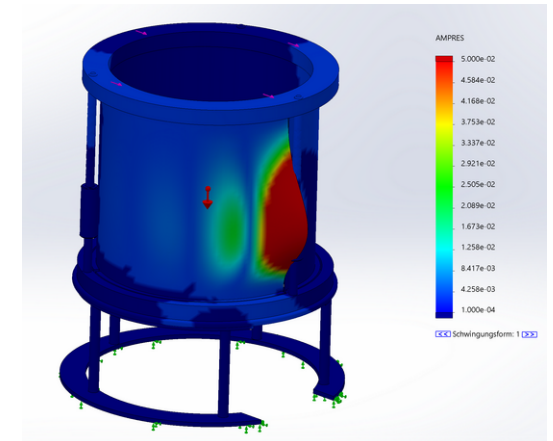
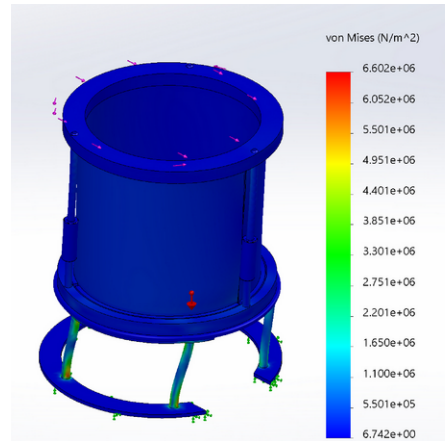
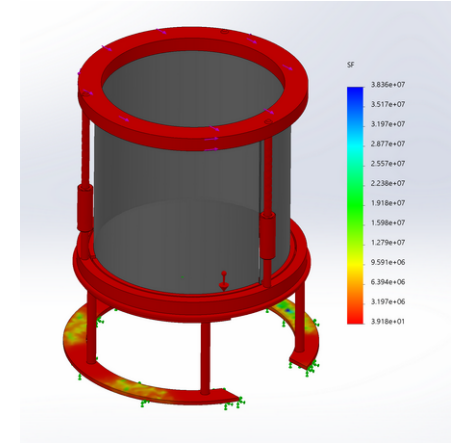
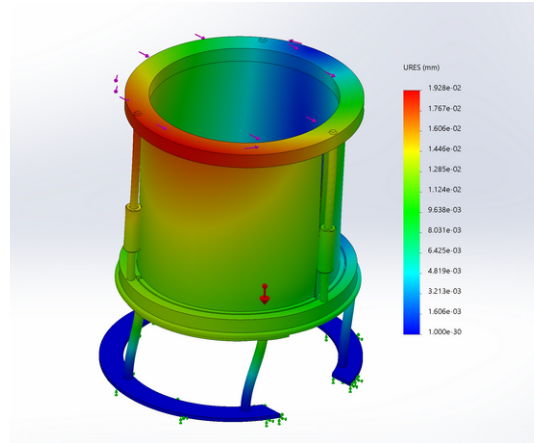
Dead Layer Estimation

- Thickness insensitive volume from Ba-133 calibration data:
 - Top and lateral source position in Marinelli beaker
 - Consistent estimates from ratio dominant lines with large energy difference and χ^2 minimization of all lines w.r.t. variable ratio sim./meas.
- Resulting values implemented in GEANT4 simulation code

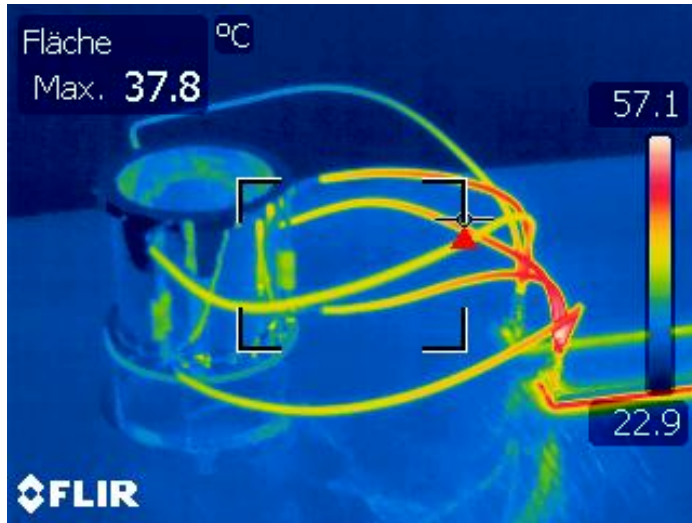


Stability Simulations

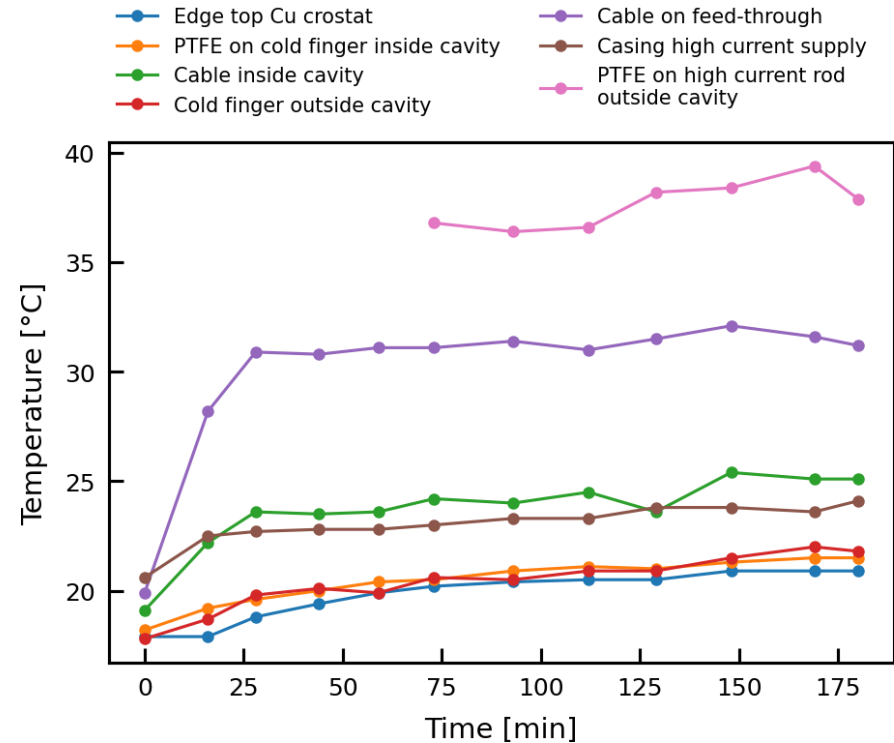
- SolidWorks stability simulations: static (stress, displacement, strain, safety factor) + buckling
- Gravity + different force / torque scenarios (shown: extreme case, i.e. gravity + 10 N lateral force top + 1 Nm torque)
- Minimum safety factor:
 - 570 (gravity only)
 - 39 (extreme case)



Thermal Tests (100 A)

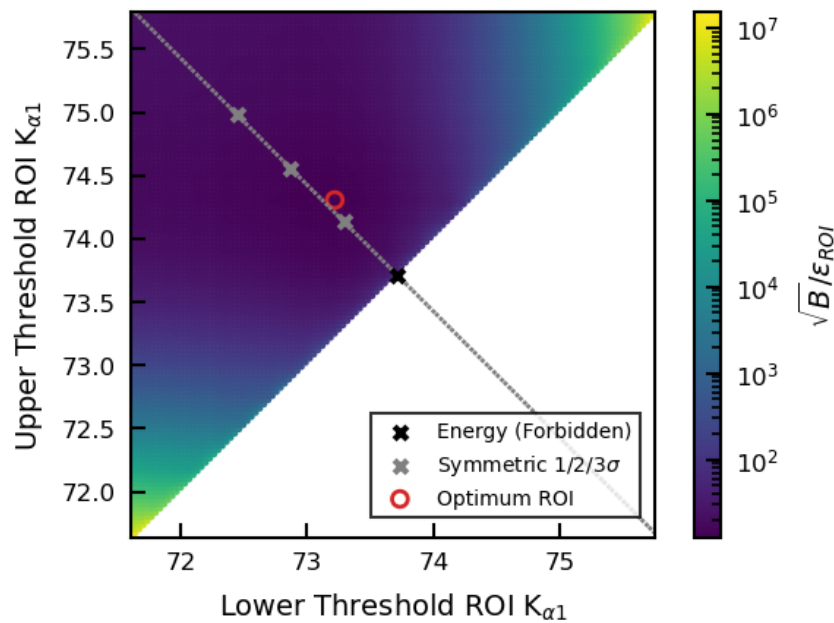


Test assembly at UZH
(FLIR camera)

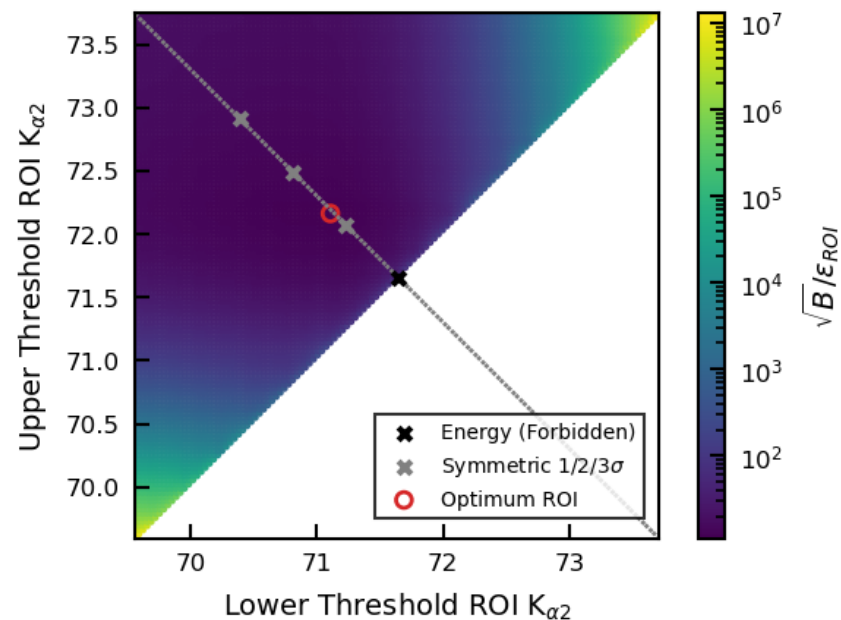


Inside Gator cavity
(contact thermometer)

Optimization ROI

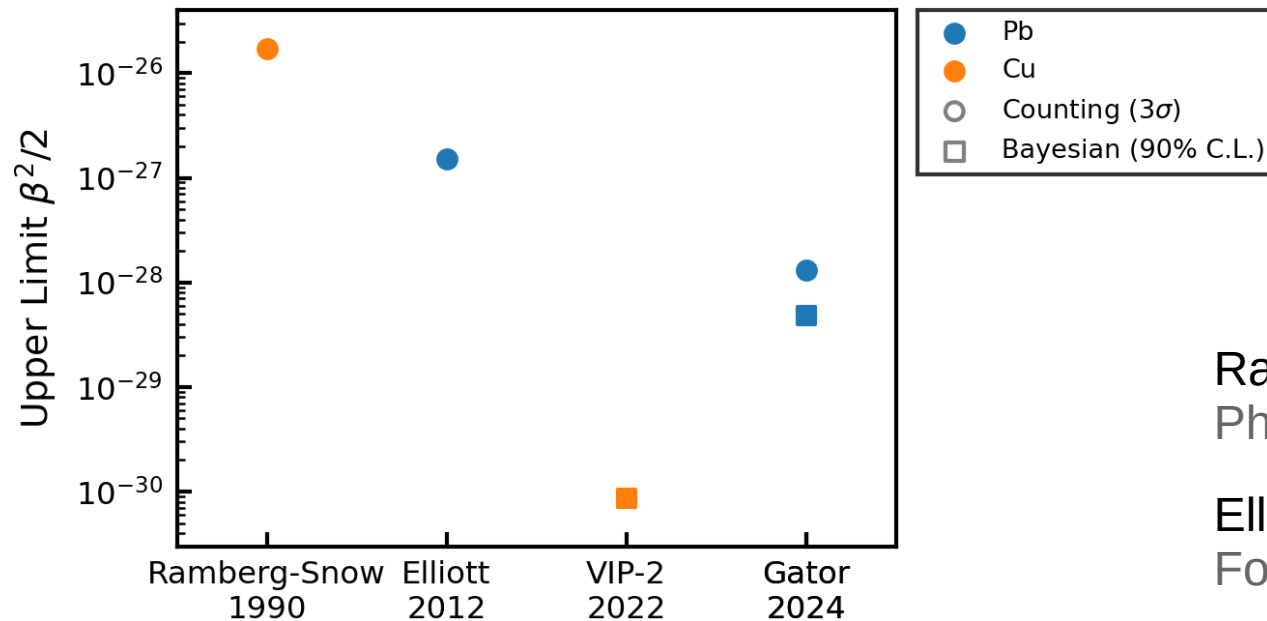


$E_{ROI1} = [73.22, 74.31]$ keV
 $\epsilon_{ROI1} = 0.7995$



$E_{ROI2} = [71.11, 72.16]$ keV
 $\epsilon_{ROI2} = 0.7895$

Comparison Other RS-Technique Experiments



Ramberg-Snow:
Phys. Lett. B 238 (1990) 438

Elliot et al.:
Found Phys 42 (2012) 1015

VIP-2:
Symmetry 14 (2022) 893